Contents lists available at ScienceDirect

Nano Energy

journal homepage: www.elsevier.com/locate/nanoen

Full paper

Self-powered mobile sterilization and infection control system

Jianjun Luo [a,b,1], Kai Han [a,b,1], Xueqiang Wu [c,1], Huaihong Cai [d], Tao Jiang [a,b], Haibo Zhou [c,*], Zhong Lin Wang [a,b,e,**]

[a] *CAS Center for Excellence in Nanoscience, Beijing Key Laboratory of Micro-nano Energy and Sensor, Beijing Institute of Nanoenergy and Nanosystems, Chinese Academy of Sciences, Beijing 100083, PR China*
[b] *School of Nanoscience and Technology, University of Chinese Academy of Sciences, Beijing 100049, PR China*
[c] *College of Pharmacy, Jinan University, Guangzhou 510632, PR China*
[d] *College of Chemistry and Materials Science, Jinan University, Guangzhou 510632, PR China*
[e] *School of Materials Science and Engineering, Georgia Institute of Technology, Atlanta, GA 30332-0245, USA*

ARTICLE INFO

ABSTRACT

With the growing mobility of the world population and the emergence of infectious diseases, the prevention and control of epidemic are particularly important for public health. Here, we report a high-performance and durable triboelectric nanogenerator (TENG) for self-powered medical health improvement. Based on a simple and effective double tribo-layers strategy, the electrical output performance of the TENG is enhanced by about 65% compared with that of traditional single tribo-layer. In addition, by introducing an automatic working mode transition design, the durability of the TENG can be greatly improved. Using the high output voltage of TENG as driven by wind, a self-powered mosquito-killing system and a self-powered ultraviolet sterilization system are further developed to control the mosquito population and bacterial reproduction for reducing the risk of disease transmission. This work not only provides a prospective strategy to improve the electrical and mechanical performance of the TENG, but also expands the application area of the self-powered system to infectious disease prevention.

1. Introduction

With the rapid development of the social economy and modern technology, interpersonal contact is becoming more and more frequent. Infectious diseases caused by bacteria and viruses could easily spread from person to person through the air, which will seriously endanger human health [1–4]. In addition, mosquito bite is the origin of numerous mosquito-borne diseases, including malaria [5,6], Japanese encephalitis [7,8], filariasis [9,10], dengue fever [11,12], and so on. Realizing high-efficiency sterilization and mosquito control can significantly reduce the risk of disease spreading and ensure public health. Currently, the common methods for mosquito-killing and sterilization are mainly divided into two categories: chemical and physical. For the chemical methods, it is inevitable that toxic chemicals may not only do harm to people's health, but also pollute the ecological environment seriously [13–16]. High-voltage mosquito-killing and ultraviolet (UV)

sterilization are two of the safe and effective physical methods. However, external power sources are indispensable for driving the relevant devices, which will have severe limitations, especially in outdoor and remote areas. Therefore, it is highly desirable to develop an environmental-friendly and maintenance-free sterilization and infection control system.

Based on the coupling effect of contact electrification and electrostatic induction, triboelectric nanogenerators (TENGs) have been recently developed into a powerful technology for converting low-frequency, distributed, and irregular mechanical energy into electricity [17]. With lots of advantages such as simple structure, low cost, high efficiency, and high output voltage [18–21], TENGs have been widely used in various fields, including micro/nano power sources, self-powered sensors, blue energy, and direct high-voltage power sources [22–27]. Therefore, the TENG technology can be effective for the new era, where huge amounts of distributed electronic devices will be

used. To expand the practical application of TENGs, power output and mechanical durability are two of the most critical parameters that need to be improved. To date, various strategies have been reported to maximize the output performance of the TENG, including improving the surface charge density, enhancing the contact intimacy, and designing innovative structures [28–33]. Meanwhile, previous researches also attempted to improve mechanical durability from the aspects of materials and structure design, such as developing robust triboelectric materials, using the rolling friction structure or non-contact structure [34–37]. However, realizing the high mechanical durability of the TENG using traditional methods will often lead to a decline in its electric output. Given this, an effective and simple strategy for simultaneously maximizing these two parameters is urgently required for practical application.

Here, we report a high-performance and durable TENG with double tribo-layers structure and automatic working mode transition. Compared with the TENG with single tribo-layer, the transferred charge and instantaneous peak power are increased by 65% and 156%, respectively. In addition, the TENG can automatically transform its working mode under the force balance between centrifugal force and gravity of the flexible rotator, which can effectively improve its stability and durability. Own to its excellent performance, the TENG is further utilized to construct a self-powered mobile sterilization and infection control system for mosquito-killing and sterilization. This work opens up new avenues for self-powered systems in infectious disease control, and will potentially promote family medical care and public health.

2. Results and discussion

2.1. Structure design of the self-powered mobile sterilization and infection control system

Fig. 1a presents the structural design of the TENG-based self-powered mobile sterilization and infection control system, which is composed of a sandwich-structured free-standing TENG as the power supply and a home-made medical health device for mosquito-killing and sterilization. For the rotary free-standing TENG (FS-TENG), a two-channel hierarchical structure is designed for simultaneously improving the output performance and realizing two independent

functions. A rotator with double-faced triboelectric layers is inserted in the middle of two PCB stators. Fig. 1b,c show the photographs of the rotator and the stator, both of which are composed of radially arrayed sectors. Give that the output characteristic of high voltage, the upper part is directly used as the high-voltage power source for mosquito eradication. Meanwhile, the lower part serves as the power supply of the ultraviolet light-emitting diode (UV-LED) module. Fig. 1d shows the photograph of the as-fabricated wind-driven TENG. By integrating with the wind cups, the FS-TENG is capable of harvesting the environmental wind energy for building up a self-powered system. The home-made medical health device mainly consists of a circular high-voltage electric network and a central UV-LED module, as shown in Fig. 1e. The UV-LED can not only attract the mosquito by utilizing its phototaxis, but also kill the bacteria by using UV irradiation. The detailed fabrication process of the TENG and home-made medical health device can be found in the Experimental section. Using the two-channel TENG for harvesting the ambient mechanical energy, self-powered mosquito-killing and sterilization could be simultaneously achieved, which is meaningful for promoting medical security level and public healthcare, as shown in Fig. 1f.

2.2. Output performance improvement of the TENG

To improve the output performance of the TENG, double tribo-layers are designed to enhance the electrostatic induction. Given that its symmetrical structure, we chose the bottom half part of the TENG for investigating the improvement mechanism and characterizing the output performance. Fig. 2a presents the output power improvement principle of the TENG with double tribo-layers. The rotator comprises of two components: a layer of epoxy glass cloth laminate sheet (FR-4) as the substrate, and two layers of FEP film attached on both sides of the FR-4 substrate as the triboelectric materials. Before assembling the TENG device, the FEP film was negatively pre-charged by rubbing with the Cu film. In the initial stage, positive charges are induced in the electrode I right below. When the rotator slides, the positive charges will flow from electrode I to electrode II until the FEP film reaches the overlapping position of electrode II. As the rotation continues, the induced positive charges will flow back in the opposite direction because of the periodic structure. This is the full cycle of the electricity
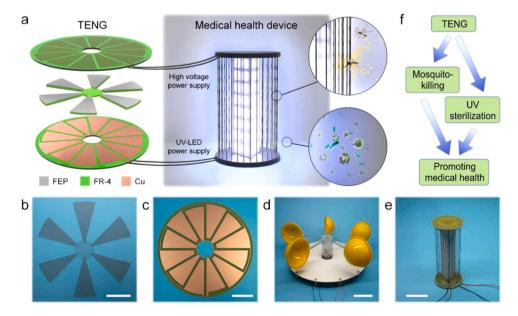

Fig. 1. Structural design and photographs of the TENG-based self-powered mobile sterilization and infection control system. (a) Schematic of the self-powered medical health system. (b,c) Photographs of the rotator (b) and stator (c) of the rotatory FS-TENG. Scale bar, 5 cm. (d) Photograph of the fabricated wind-driven TENG device. Scale bar, 6 cm. (e) Photograph of the home-made medical health device. Scale bar, 3 cm. (f) Flow chart of the self-powered sterilization and infection control system.
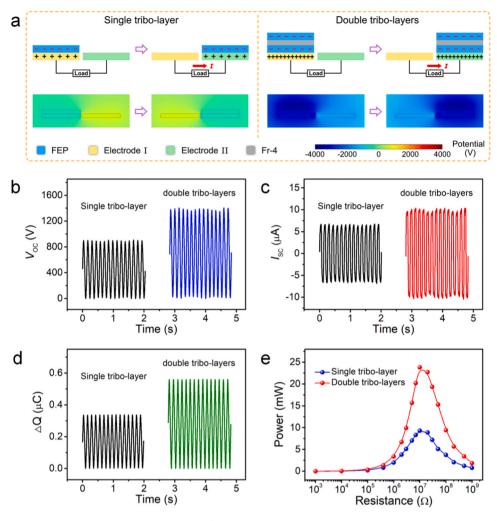
Fig. 2. Output performance improvement of the TENG. (a) Schematic illustration of the output performance improvement mechanism and potential simulation by COMSOL to elucidate the improvement mechanism. (b-e) Comparison of the open-circuit voltage (b), short-circuit current (c), transferred charge (d), and peak power (e) between TENGs with single tribo-layer and double tribo-layers.
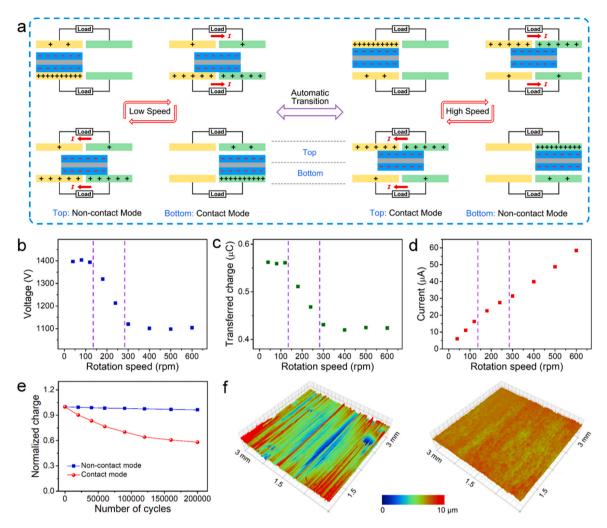
generation process. Compared with the TENG with single tribo-layer, it has higher surface charge density, which can induce more positive triboelectric charges in the bottom electrode for improving the output performance. For a better understanding of the proposed mechanism, corresponding potential distributions under the open-circuit condition are also simulated.

To quantitatively evaluate the improvement mechanism, we subsequently measured the output performance of the TENGs fabricated with single tribo-layer and double tribo-layers. The open-circuit voltage (V_{OC}), short-circuit current (I_{SC}), and transferred charge ($\triangle Q$) of the TENG fabricated with single tribo-layer are shown in Fig. 2b-d, with peaks of 900 V, 6.7 µA, and 0.34 µC, respectively. When using the tribo-layers for fabricating TENG, its V_{OC}, I_{SC}, and $\triangle Q$ can be improved to 1400 V, 10.4 µA, and 0.56 µC, under the same rotation speed of 75 rpm/min. By comparing their output charge, TENG with double tribo-layers is 65% higher than that of single tribo-layer. To further evaluate the effective output power improvement, the output current of the TENGs was measured with various resistances applied as the external load, under the rotation speed of 600 rpm/min. The relationship between the output current and the resistance is plotted in Fig. S1. As shown in Fig. 2e, the maximum peak output power of 23.8 mW can be achieved under the external load of 10 MΩ, which is 2.6 times of that for the TENG with single tribo-layer.

2.3. Mechanical durability improvement of the TENG

For practical applications that need to scavenge high-frequency mechanical energy for an extended period, such as airflow, rotational tires, and water flow, wear and tear of tribo-material will inevitably occur, which could severely reduce the output power of the TENG or even damage the device. To further improve the mechanical durability of the TENG, we designed an automatic mode transition structure by utilizing the force balance between centrifugal force and gravity of the flexible rotator in different rotation speeds. The working mechanism of automatic mode transition is schematically illustrated in Fig. 3a, including top and bottom parts of free-standing TENGs. At low rotation speed, gravity is dominant in the resultant force of each rotator blade. Thus, each blade will stay in bending state and contact with bottom electrodes due to its flexibility, while separate with top electrodes. In this case, the top TENG works in non-contact mode, and the bottom TENG works in contact mode. As the rotation speed continues to increase, the rotator blade begins to separate with bottom electrodes since its centrifugal force gradually increases. When its centrifugal force becomes much larger than the gravity at high rotation speed, the blades will then overcome the gravity and completely separate with the bottom electrodes, resulting in the working mode conversion of top and bottom TENGs. Real-time operating states of the rotator in low and high rotation speed are shown in Fig. S2 and Movie S1, S2, Supplementary material.

Supplementary material related to this article can be found online at

Fig. 3. Durability improvement of the TENG. (a) Schematic illustration of the automatic working mode transition between the upper and lower parts of the TENG triggered by the rotation speed. (b-d) Open-circuit voltage (b), transferred charge (c), and short-circuit current (d) of the TENG under different rotation speeds. (e) Robustness investigation of the TENG in different working modes. (f) 3D interferometer images of wear traces on the FEP films in contact mode and non-contact mode after 20,000 working cycles.
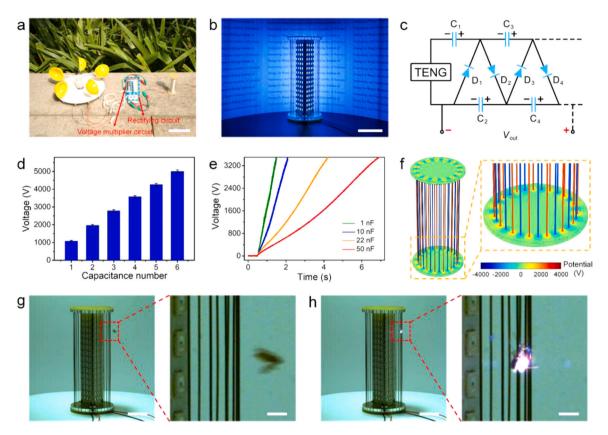
doi:10.1016/j.nanoen.2021.106313.

Considering the symmetrical structure of this automatic mode transition design, we choose the bottom part of free-standing TENG for experimentally investigating its electrical performance and mechanical durability. As shown in Fig. 3b-d, nine sets of output voltage, transferred charge, and output current were systematically measured under a variety of rotation speeds. Fig. 3b shows the relationship between the output voltage and rotation speed, which can be divided into three regions. In the first region with rotation speed less than 120 rpm, the output voltage remains at a constant value of about 1400 V because of the full contact between the flexible rotator and bottom electrodes. In the transition region with rotation speed between 120 rpm and 300 rpm, the output voltage rapidly decreases from 1400 V to 1100 V with the increase of rotation speed, which is because the rotator gradually separates with the stator. Subsequently, when the rotation speed increases to more than 300 rpm, the output voltage reaches another stable value of about 1100 V due to the complete separation between the rotator and stator. The output voltage only decreases by about 22% after the working mode transition, demonstrating its excellent electric output. The transferred charge shows a similar variation trend, reducing from 0.56 μC in contact mode to 0.42 μC in non-contact mode (Figs. 3c and S3, Supplementary material). Fig. 3d shows the measurement result of output current under different rotation speeds. Unlike the output voltage and transferred charge, the output current is mainly affected by the

charge transfer rate. Thus, it can be seen that the increase of rotation speed leads to a monotonic increasing of output current from 6 μA to 58 μA. The detailed variation trend of the output current is shown in Fig. S4, Supplementary material. To verify the feasibility of our structural design, the electrical performance of the upper part of the TENG was also investigated (Fig. S5, Supplementary material).

Benefit from this mode transition design, the robustness of the TENG can be greatly improved. As shown in Fig. 3e, there is no observable output degradation after 20,000 working cycles when operated in the non-contact free-standing mode. However, an obvious degradation of up to 42% was observed for the contact sliding mode. Fig. 3f shows the surface wear traces of the FEP rotators in two working modes after 20,000 working cycles. Compared to that of the contact mode TENG, the mechanical wear of the non-contact mode TENG is negligible, demonstrating its excellent long-term durability.

2.4. Self-powered mosquito-killing system

In order to prevent the spread of mosquito-borne diseases, it is of great importance to developing an environmental-friendly method for controlling the mosquito population. As shown in Fig. 4a, a TENG-based self-powered mosquito-killing system was built by integrating with a home-made mosquito-killing lamp using 365 nm UVA light. It has been reported that this kind of UVA light with a peak wavelength of 365 nm

Fig. 4. Self-powered mosquito-killing system. (a) Photograph of the self-powered mosquito-killing system. Scale bar, 10 cm. (b) Photograph of 180 UVA-LEDs in the home-made mosquito-killing lamp that are directly powered by the TENG. Scale bar, 3 cm. (c) Electric circuit diagram of the voltage multiplier circuit for converting AC to DC with high voltage. (d) Voltage variation of the TENG using voltage multiplier circuits with different numbers of capacitors. (e) Voltage charging curves of the TENG using voltage multiplier circuits with different capacitors. (f) Potential simulation of the home-made mosquito-killing lamp powered by the TENG. (g-h) High-speed camera photographs showing the mosquito-killing process of before (g) and after (h) contacting with the high-voltage electric grid. Scale bar, 3 cm for the standard view, 3 mm for the enlarged view.

can effectively attract mosquitos [38,39]. The wind-driven TENG is capable of harvesting environmental energy and simultaneously powering the high-voltage electric network and trapping light. The spectrum diagram of the UVA-LED is measured in Fig. S5, Supplementary material. 180 UVA-LEDs can be easily lighted up by the TENG through a rectifying circuit (Fig. 4b and Movie S3, Supplementary material). Although the TENG itself has shown excellent high-voltage characteristics, higher output voltage and energy are required for efficient mosquito-killing. To tackle this problem, a voltage multiplier circuit containing diodes and capacitors was further used, as shown in Fig. 4c. For better mosquito-killing performance, output voltage, energy, and charging period are critical parameters. Fig. 4d shows the relationship between the output voltage and capacitance number, indicating that the voltage multiplier circuit can effectively improve the output voltage of the TENG. Thanks to the high output power of the TENG, the self-powered electric grid can rapidly produce a high voltage, demonstrating its high efficiency. It can be seen that the charge time from 0 V to 3500 V is less than 7 s even for the five-stage voltage multiplier circuit with the capacitance of 50 nF, which could produce enough energy for killing mosquitos (Fig. 4e). Considering its high output power and short charging period, the fabricated TENG-based self-powered system exhibits great potential for practical application. The corresponding simulation of potential distribution between two poles in the electric grid by COMSOL is presented in Fig. 4f.

Supplementary material related to this article can be found online at doi:10.1016/j.nanoen.2021.106313.

To experimentally verify the feasibility of the TENG-based self-powered system, we further use it to attract the mosquitos by utilizing their phototaxis and record the process with a high-speed camera.

Fig. 4g, h shows the instantaneous states of the mosquito before and after getting an electric shock. When the mosquito contacts with the electric grid, an obvious electric spark can be seen. The complete mosquito-killing process captured by the high-speed camera is shown in Movie S4, Supplementary material. These results demonstrate the promising anti-mosquito potential of the self-powered mosquito-killing system in the outdoor environment.
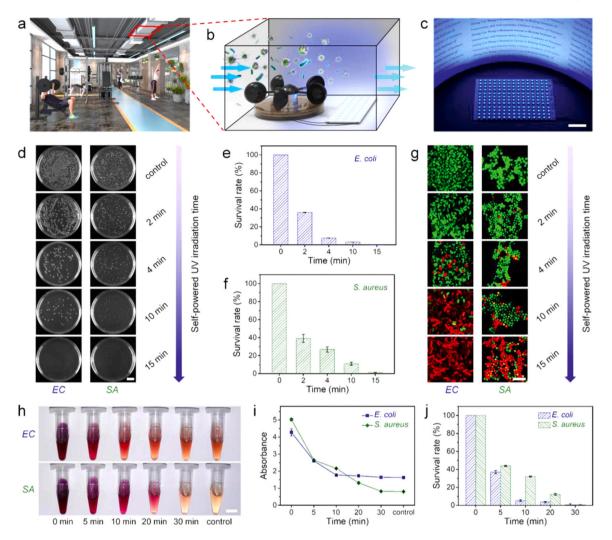
Supplementary material related to this article can be found online at doi:10.1016/j.nanoen.2021.106313.

2.5. Self-powered UV sterilization system

Considering many infectious diseases spread easily through the air, it will be a promising way to utilize environmental energy for reducing the risk of infectious disease transmission. Fig. 5a depicts the conceptional application of the TENG for scavenging indoor environmental energy for self-powered UV sterilization. The TENG can be installed in the air conditioner pipe to harvest the wind energy for powering UVC-LEDs, which has been reported to be effective for disinfection and sterilization [40,41]. Fig. 5b illustrates the enlarged view inside the air conditioner pipe and the working mechanism for self-powered sterilization. After UV irradiation treatment, the bacterial content in the air could be reduced. The peak wavelength of the UVC-LED is 277 nm, as shown in Fig. S6, Supplementary material. 180 UVC-LEDs can be easily lighted up by the TENG, demonstrating the feasibility of killing bacteria (Fig. 5c and Movie S5, Supplementary material).

Supplementary material related to this article can be found online at doi:10.1016/j.nanoen.2021.106313.

To verify the universal sterilization effect of the self-powered

Fig. 5. Self-powered UV sterilization system. (a) A proposed conceptual application of the wind-driven TENG using for self-powered UV sterilization in the indoor environment. (b) Enlarged view of the air conditioner pipe where the TENG could harvest the wind energy for driving UVC-LEDs. (c) Photograph of 180 UVC-LEDs that are directly powered by the TENG. Scale bar, 2 cm. (d) Photographs of *E. coli* (*EC*) and *S. aureus* (*SA*) colonies under various irradiation times. Scale bar, 1 cm. (e-f) Survival rates of *E. coli* (e) and *S. aureus* (f) at different treatment times by counting the colonies of (d). (g) Enlarged fluorescent images of live (green) and dead (red) bacterial cells under various irradiation times. Scale bar, 5 μm. (h) Photographs of bacterial solutions in MTT assay under various irradiation times. Scale bar, 1 cm. (i) Absorbance curves of bacterial solutions in MTT assay. (j) Calculated survival rates of bacteria in MTT assay using the data retrieved from (i). (For interpretation of the references to colour in this figure legend, the reader is referred to the web version of this article.)

sterilization system, *E. coli* and *S. aureus* were treated by self-powered UV irradiation for 0–15 min, and the results of sterilization are shown in Fig. 5d. It is worth noting that the colony counts of the bacteria decrease markedly with the increase of irradiation time and finally disappear in 15 min. Then, the change of survival rate with the irradiation time was also calculated by counting the colonies from Fig. 5d, and the results for *E. coli* and *S. aureus* were shown in Fig. 5e and f, respectively. They both showed a dramatic change with the irradiation time, while *S. aureus* has a more tender drop line, which may suggest that *S. aureus* is more resistant to UV light than *E. coli*. Furthermore, the survival of bacteria under irradiation of UVC-LEDs was also assessed by using Live (green)/Dead (red) dual-color fluorescent staining (Fig. 5g). The result showed that *E. coli* was completely killed in 15 min while part of *S. aureus* was still alive, which was consistent with the result of Fig. 5d-f. Finally, the effect of self-powered UVC-LEDs irradiation on the bacteria was explored by MTT assay (Fig. 5h), and the corresponding change of absorbance and the calculated survival rate with various irradiation times were shown in Fig. 5i and j, respectively. The results indicated that both bacteria completely lost their vitality in 30 min even after 1 h incubation flowing with the irradiation. Overall, the

antibacterial results indicate that the self-powered UV sterilization system possesses a superior bactericidal ability and can greatly prevent the airborne transmission of bacteria in the indoor environment.

3. Conclusion

In conclusion, we developed a high-performance and durable triboelectric nanogenerator for self-powered mobile sterilization and infection control system. The high output of the TENG was realized by designing a simple and effective double tribo-layers structure, with significant enhancements of 65% and 156% in transferred charges and instantaneous peak power, respectively. Furthermore, by introducing the automatic working mode transition structure, the stability and durability of the TENG can be greatly improved. As a demonstration, the TENG is adopted for constructing a self-powered mosquito-killing system, which is composed of a TENG-driven trapping light and a high-voltage electric network. Furthermore, a self-powered UV sterilization system was also developed to inhibit bacterial reproduction in the indoor air environment. This research will broaden the application of TENG in self-powered medical health devices and disease transmission

control, and may promote family medical care and public health.

4. Experimental section

4.1. Fabrication of the rotary sliding FS-TENG

The rotary sliding FS-TENG mainly consists of two stators and a rotator. The rotator was coaxially placed between the two stators. For the stator, a custom-made disc-shaped PCB with a diameter of 23 cm was applied as the supporting substrate. 6 pairs of Cu electrodes with an interspace of 5 mm on the PCB surface were regarded as the triboelectric and electrode layers. A circular region with a diameter of 40 mm was cut in the center of the PCB board for the space of the drive shaft. For the rotator, a flexible blade-shaped FR-4 board with a diameter of 20 cm and thickness of 0.3 mm was used as the substrate. Then a layer of FEP film with a thickness of 25 μm was adhered on the upper and lower surfaces of the FR-4 substrate as the free-standing triboelectric layer.

4.2. Fabrication of the medical health device

The home-made medical health device is composed of two parts: a high-voltage electric network and a UV-LED module (APT Electronics Co., Ltd., China). For the high-voltage network, a custom-made disc-shaped PCB with a diameter of 43 mm was applied as the supporting substrate. 30 steel wires with a diameter 0.3 mm and a separation distance of about 0.36 mm were installed along the edge of the PCB. For the UV-LED module, 180 UV-LEDs were connected in series and evenly distributed across the surface of the prismatic PCB board.

4.3. Bacterial culture

E. coli (ATCC 25922) and *S. aureus* (ATCC 25923) were cultured in Luria-Bertani and Mueller-Hinton broth medium respectively in a shaking incubator (300 rpm) at 37 °C and harvested at the logarithmic growth phase by centrifugation at 4000 *g* for 10 min. After washing with PBS buffer three times, the bacteria were resuspended in PBS for further use. The concentration of bacteria was assessed by measuring the optical density at 600 nm (OD_{600}) through a microplate reader.

4.4. Antibacterial experiments

E. coli (ATCC 25922) and *S. aureus* (ATCC 25923) were diluted by sterilized 0.9 wt% NaCl solution and coated on sterilized nutrient agar plates in Petri dishes, which were then irradiated by the self-powered UVC-LEDs for 2, 4, 10, and 15 min, respectively. The distance between the UVC-LEDs and Petri dishes was 15 mm.

4.5. Live/dead staining assay

The viability of bacteria was qualitatively assessed using a Live/Dead® *Bac*light™ bacterial viability kit (Molecular Probes, Invitrogen), and all experiments were performed according to the manufacturer's instructions. Bacteria (OD_{600} 0.5) were irradiated by the self-powered UVC-LEDs for 2, 4, 10, and 15 min, respectively. After washing with sterilized 0.9 wt% NaCl solution, the bacteria (1 mL) were incubated with 3 μL of the mixture of 1.67 mM SYTO 9 dye (green fluorescence) and 10 mM propidium iodide dye (red fluorescence) for 15 min in the dark. Then the samples were imaged using a laser scanning confocal microscope.

4.6. MTT assay

MTT reagent was prepared by dissolving 20 mg of 3-(4,5-dimethylthiazol-2-yl)-2,5-diphenyltetrazolium bromide (MTT) (Sigma-Aldrich) in 4 mL PBS and sterilized through 0.22 μm membrane filters. The diluted bacteria solutions (OD_{600} 0.5) were irradiated by the self-

powered UVC-LEDs for 5, 10, 30, and 30 min respectively. Then 1 mL of samples were incubated with 100 μL 5 mg/mL MTT in the shaking incubator at 37 °C for 2 h, while 1 mL of bacteria was boiled to death before incubation treating as a control group. Finally, 200 μL incubated bacteria was dissolved in 500 μL DMSO, and the absorbance values at 517 nm were recorded using a spectrophotometer to calculate the survival rate of bacteria.

4.7. Characterization and measurements

The rotary sliding FS-TENG was driven by a motor (PC MOTOR) with adjustable speed. The open-circuit voltage was measured using an electrostatic voltmeter (Trek 347). A programmable electrometer (Keithley 6514) was used to test the short-circuit current and transferred charge. An optical profilometer (Contour GTK, Bruker) was used to characterize the morphologies of the FEP films. The fluorescence images of stained bacteria were captured by a Zeiss 880 confocal laser scanning microscope (ZEISS, North Ryde). A spectrophotometer (Nano-Photometer® N50, Implen) was used to measure the absorbance value of bacteria solutions.

CRediT authorship contribution statement

Jianjun Luo: Conceptualization, Investigation, Writing - original draft, Writing - review & editing. **Kai Han:** Investigation. **Xueqiang Wu:** Investigation. **Huaihong Cai:** Experiment. **Tao Jiang:** Experiment. **Haibo Zhou:** Supervision, Writing - review & editing. **Zhong Lin Wang:** Supervision, Conceptualization, Writing - review & editing.

Declaration of Competing Interest

The authors declare that they have no known competing financial interests or personal relationships that could have appeared to influence the work reported in this paper.

Acknowledgements

Appendix A. Supporting information

Supplementary data associated with this article can be found in the online version at doi:10.1016/j.nanoen.2021.106313.

References

[1] L. Hall-Stoodley, J.W. Costerton, P. Stoodley, Bacterial biofilms: from the natural environment to infectious diseases, Nat. Rev. Microbiol. 2 (2004) 95–108.
[2] K.E. Jones, N.G. Patel, M.A. Levy, A. Storeygard, D. Balk, J.L. Gittleman, P. Daszak, Global trends in emerging infectious diseases, Nature 451 (2008) 990–994.
[3] M.S. Cohen, Y.Q. Chen, M. McCauley, T. Gamble, M.C. Hosseinipour, N. Kumarasamy, J.G. Hakim, J. Kumwenda, B. Grinsztejn, J.H.S. Pilotto, S. V. Godbole, S. Mehendale, S. Chariyalertsak, B.R. Santos, K.H. Mayer, I.F. Hoffman, S.H. Eshleman, E. Piwowar-Manning, L. Wang, J. Makhema, L.A. Mills, G. de Bruyn, I. Sanne, J. Eron, J. Gallant, D. Havlir, S. Swindells, H. Ribaudo, V. Elharrar, D. Burns, T.E. Taha, K. Nielsen-Saines, D. Celentano, M. Essex, T.R. Fleming, H. S. Team, Prevention of HIV-1 infection with early antiretroviral therapy, N. Engl. J. Med. 365 (2011) 493–505.
[4] D.W. Wang, B. Hu, C. Hu, F.F. Zhu, X. Liu, J. Zhang, B.B. Wang, H. Xiang, Z. S. Cheng, Y. Xiong, Y. Zhao, Y.R. Li, X.H. Wang, Z.Y. Peng, Clinical characteristics

of 138 hospitalized patients with 2019 novel coronavirus-infected pneumonia in Wuhan, China, JAMA - J. Am. Med. Assoc. 323 (2020) 1061–1069.

[5] C.M. Cirimotich, Y. Dong, A.M. Clayton, S.L. Sandiford, J.A. Souza-Neto, M. Mulenga, G. Dimopoulos, Natural microbe-mediated refractoriness to *Plasmodium* infection in *Anopheles gambiae*, Science 332 (2011) 855–858.

[6] H. Ranson, R. N'Guessan, J. Lines, N. Moiroux, Z. Nkuni, V. Corbel, Pyrethroid resistance in African anopheline mosquitoes: what are the implications for malaria control? Trends Parasitol. 27 (2011) 91–98.

[7] J.S. Mackenzie, D.J. Gubler, L.R. Petersen, Emerging flaviviruses: the spread and resurgence of Japanese encephalitis, West Nile and dengue viruses, Nat. Med. 10 (2004) S98–S109.

[8] A.F. van den Hurk, S.A. Ritchie, J.S. Mackenzie, Ecology and geographical expansion of Japanese Encephalitis Virus, Annu. Rev. Entomol. 54 (2009) 17–35.

[9] R.M.R. Ramzy, M. El Setouhy, H. Helmy, E.S. Ahmed, K.M. Abd Elaziz, H.A. Farid, W.D. Shannon, G.J. Weil, Effect of yearly mass drug administration with diethylcarbamazine and albendazole on bancroftian filariasis in Egypt: a comprehensive assessment, Lancet 367 (2006) 992–999.

[10] M.J. Bockarie, E.M. Pedersen, G.B. White, E. Michael, Role of vector control in the global program to eliminate lymphatic filariasis, Annu. Rev. Entomol. 54 (2009) 469–487.

[11] M.G. Guzman, S.B. Halstead, H. Artsob, P. Buchy, F. Jeremy, D.J. Gubler, E. Hunsperger, A. Kroeger, H.S. Margolis, E. Martinez, M.B. Nathan, J.L. Pelegrino, S. Cameron, S. Yoksan, R.W. Peeling, Dengue: a continuing global threat, Nat. Rev. Microbiol. 8 (2010) S7–S16.

[12] M.G. Guzman, E. Harris, Dengue, Lancet 385 (2015) 453–465.

[13] R.S. Davis, R.K.D. Peterson, P.A. Macedo, An ecological risk assessment for insecticides used in adult mosquito management, Integr. Environ. Assess. Manag. 3 (2007) 373–382.

[14] L.S. Nerio, J. Olivero-Verbel, E. Stashenko, Repellent activity of essential oils: a review, Bioresour. Technol. 101 (2010) 372–378.

[15] J.L. Zhao, G.G. Ying, Y.S. Liu, F. Chen, J.F. Yang, L. Wang, Occurrence and risks of triclosan and triclocarban in the Pearl River system, South China: from source to the receiving environment, J. Hazard. Mater. 179 (2010) 215–222.

[16] P. Liu, H. Zhang, Y. Feng, F. Yang, J. Zhang, Removal of trace antibiotics from wastewater: a systematic study of nanofiltration combined with ozone-based advanced oxidation processes, Chem. Eng. J. 240 (2014) 211–220.

[17] F.R. Fan, Z.Q. Tian, Z.L. Wang, Flexible triboelectric generator!, Nano Energy 1 (2012) 328–334.

[18] Z.L. Wang, J. Chen, L. Lin, Progress in triboelectric nanogenerators as a new energy technology and self-powered sensors, Energy Environ. Sci. 8 (2015) 2250–2282.

[19] B. Meng, W. Tang, Z.H. Too, X.S. Zhang, M.D. Han, W. Liu, H.X. Zhang, A transparent single-friction-surface triboelectric generator and self-powered touch sensor, Energy Environ. Sci. 6 (2013) 3235–3240.

[20] J. Luo, Z.L. Wang, Recent progress of triboelectric nanogenerators: from fundamental theory to practical applications, EcoMat 2 (2020), e12059.

[21] R. Hinchet, H.J. Yoon, H. Ryu, M.K. Kim, E.K. Choi, D.S. Kim, S.W. Kim, Transcutaneous ultrasound energy harvesting using capacitive triboelectric technology, Science 365 (2019) 491–494.

[22] B.N. Chandrashekar, B. Deng, A.S. Smitha, Y.B. Chen, C.W. Tan, H.X. Zhang, H. L. Peng, Z.F. Liu, Roll-to-roll green transfer of CVD graphene onto plastic for a transparent and flexible triboelectric nanogenerator, Adv. Mater. 27 (2015) 5210–5216.

[23] K. Parida, G. Thangavel, G.F. Cai, X.R. Zhou, S. Park, J.Q. Xiong, P.S. Lee, Extremely stretchable and self-healing conductor based on thermoplastic elastomer for all-three-dimensional printed triboelectric nanogenerator, Nat. Commun. 10 (2019) 2158.

[24] J. Luo, W. Tang, F.R. Fan, C. Liu, Y. Pang, G. Cao, Z.L. Wang, Transparent and flexible self-charging power film and its application in a sliding unlock system in touchpad technology, ACS Nano 10 (2016) 8078–8086.

[25] J. Luo, W. Gao, Z.L. Wang, The triboelectric nanogenerator as an innovative technology toward intelligent sports, Adv. Mater. 33 (2021) 2004178.

[26] X. Yang, L. Xu, P. Lin, W. Zhong, Y. Bai, J. Luo, J. Chen, Z.L. Wang, Macroscopic self-assembly network of encapsulated high-performance triboelectric nanogenerators for water wave energy harvesting, Nano Energy 60 (2019) 404–412.

[27] H.S. Kim, D.Y. Kim, J.E. Kim, J.H. Kim, D.S. Kong, G. Murillo, G.H. Lee, J.Y. Park, J.H. Jung, Ferroelectric-Polymer-Enabled Contactless Electric Power Generation in Triboelectric Nanogenerators, Adv. Funct. Mater. 29 (2019) 1905816.

[28] F.R. Fan, J. Luo, W. Tang, C. Li, C. Zhang, Z.Q. Tian, Z.L. Wang, Highly transparent and flexible triboelectric nanogenerators: performance improvements and fundamental mechanisms, J. Mater. Chem. A 2 (2014) 13219–13225.

[29] C.K. Jeong, K.M. Baek, S.M. Niu, T.W. Nam, Y.H. Hur, D.Y. Park, G.T. Hwang, M. Byun, Z.L. Wang, Y.S. Jung, K.J. Lee, Topographically-designed triboelectric nanogenerator via block copolymer self-assembly, Nano Lett. 14 (2014) 7031–7038.

[30] P. Cheng, H. Guo, Z. Wen, C. Zhang, X. Yin, X. Li, D. Liu, W. Song, X. Sun, J. Wang, Z.L. Wang, Largely enhanced triboelectric nanogenerator for efficient harvesting of water wave energy by soft contacted structure, Nano Energy 57 (2019) 432–439.

[31] L. Cheng, Q. Xu, Y.B. Zheng, X.F. Jia, Y. Qin, A self-improving triboelectric nanogenerator with improved charge density and increased charge accumulation speed, Nat. Commun. 9 (2018) 3773.

[32] W. Liu, Z. Wang, G. Wang, G. Liu, J. Chen, X. Pu, Y. Xi, X. Wang, H. Guo, C. Hu, Z. L. Wang, Integrated charge excitation triboelectric nanogenerator, Nat. Commun. 10 (2019) 1426.

[33] Y. Bai, L. Xu, S.Q. Lin, J. Luo, H. Qin, K. Han, Z.L. Wang, Charge pumping strategy for rotation and sliding type triboelectric nanogenerators, Adv. Energy Mater. 10 (2020) 2000605.

[34] J. Luo, Z. Wang, L. Xu, A.C. Wang, K. Han, T. Jiang, Q. Lai, Y. Bai, W. Tang, F. R. Fan, Z.L. Wang, Flexible and durable wood-based triboelectric nanogenerators for self-powered sensing in athletic big data analytics, Nat. Commun. 10 (2019) 5147.

[35] L. Lin, Y. Xie, S. Niu, S. Wang, P. Yang, Z.L. Wang, Robust triboelectric nanogenerator based on rolling electrification and electrostatic induction at an instantaneous energy conversion efficiency of similar to 55%, ACS Nano 9 (2015) 922–930.

[36] L. Zhou, D. Liu, Z. Zhao, S. Li, Y. Liu, L. Liu, Y. Gao, Z.L. Wang, J. Wang, Simultaneously enhancing power density and durability of sliding-mode triboelectric nanogenerator via interface liquid lubrication, Adv. Energy Mater. 10 (2020), 2002920.

[37] J. Chen, H. Guo, C. Hu, Z.L. Wang, Robust triboelectric nanogenerator achieved by centrifugal force induced automatic working mode transition, Adv. Energy Mater. 10 (2020) 2000886.

[38] E.P. Mwanga, H.S. Ngowo, S.A. Mapua, A.S. Mmbando, E.W. Kaindoa, K. Kifungo, F.O. Okumu, Evaluation of an ultraviolet LED trap for catching Anopheles and Culex mosquitoes in south-eastern Tanzania, Parasites Vectors 12 (2019) 418.

[39] D.A.H. Peach, E. Ko, A.J. Blake, G. Gries, Ultraviolet inflorescence cues enhance attractiveness of inflorescence odour to Culex pipiens mosquitoes, PLoS One 14 (2019), e0217484.

[40] W.A.M. Hijnen, E.F. Beerendonk, G.J. Medema, Inactivation credit of UV radiation for viruses, bacteria and protozoan (oo)cysts in water: a review, Water Res. 40 (2006) 3–22.

[41] M. Gagol, A. Przyjazny, G. Boczkaj, Wastewater treatment by means of advanced oxidation processes based on cavitation - A review, Chem. Eng. J. 338 (2018) 599–627.

Dr. Jianjun Luo received his B.S. degree in Applied Chemistry from Jinan University in 2013, and his Ph.D. degree in Condensed Matter Physics from University of Chinese Academy of Sciences in 2018. He is now a postdoctoral fellow in Beijing Institute of Nanoenergy and Nanosystems, Chinese Academy of Sciences, under the supervision of Prof. Zhong Lin Wang. His research interests include triboelectric nanogenerators, self-powered systems and supercapacitors.

Dr. Kai Han received his B.E. degree in Macromolecular Materials and Engineering from Qingdao University in 2012, M.E. degree in Applied Chemistry from Shanghai University in 2015, and Ph.D. degree in Condensed Matter Physics from University of Chinese Academy of Sciences in 2020. He is now a postdoctoral fellow in Jinan University and a visiting fellow in Beijing Institute of Nanoenergy and Nanosystems, Chinese Academy of Sciences, under the supervision of Prof. Zhong Lin Wang. His research interests include triboelectric nanogenerators, self-powered electrochemistry and systems.

Xueqiang Wu is presently pursuing his Ph.D. degree in College of Pharmacy, Jinan University, China. His current research focuses on the detection and inhibition of human monoamine oxidase B and its possible application in the development of inhibitor-type drugs.

Dr. Tao Jiang is a professor in the Beijing Institute of Nanoenergy and Nanosystems, Chinese Academy of Sciences. He received his bachelor and Ph.D. degrees from School of Materials Science and Engineering, in 2008 and 2014, respectively, from East China University of Science and Technology. After graduation, he worked in the Beijing Institute of Nanoenergy and Nanosystems as a postdoctoral research fellow. His research interests are the theoretical studies of triboelectric nanogenerators, and practical applications in blue energy harvesting.

Prof. Haibo Zhou received his Ph.D. degree from Technical University of Munich, Germany, in 2014, under the tutelage of Professor Reinhard Niessner, Director of the Institute of Hydrochemistry and the Chair of Analytical Chemistry. Currently, he is a professor in Jinan University. His main research areas include pharmaceutical analysis, biopharmaceutical micro-nanosensor devices (chromatography, surface-enhanced Raman spectroscopy, fluorescence, chemiluminescence), and biomedical diagnostic methods based on nano properties.

Prof. Zhong Lin Wang received his Ph.D. degree from Arizona State University in physics. He now is the Hightower Chair in Materials Science and Engineering, Regents' Professor at Georgia Tech, the chief scientist and director of the Beijing Institute of Nanoenergy and Nanosystems, Chinese Academy of Sciences. Prof. Wang has made original and innovative contributions to the synthesis, discovery, characterization and understanding of fundamental physical properties of oxide nanobelts and nanowires, as well as applications of nanowires in energy sciences, electronics, optoelectronics and biological science. His discovery and breakthroughs in developing nanogenerators establish the principle and technological road map for harvesting mechanical energy from environmental and biological systems for powering personal electronics. His research on self-powered nanosystems has inspired the worldwide efforts in academia and industry for studying energy for micro-nano-systems, which is now a distinct disciplinary in energy research and future sensor networks. He coined and pioneered the fields of piezotronics and piezophototronics by introducing piezoelectric potential gated charge transport process in fabricating new electronic and optoelectronic devices.